Diffusion-Occ: 3D Point Cloud Completion via Occupancy Diffusion

Guoqing Zhang*, **Jian Liu***

Harbin Institute of Technology

Abstract

Point clouds are crucial for capturing three-dimensional data but often suffer from incompleteness due to limitations such as resolution and occlusion. Traditional methods typically rely on point-based approaches within discriminative frameworks for point cloud completion. In this paper, we introduce **Diffusion-Occ**, a novel framework for Diffusion Point Cloud Completion. Diffusion-Occ utilizes a two-stage coarse-to-fine approach. In the first stage, the Coarse Density Voxel Prediction Network (CDNet) processes partial points to predict coarse density voxels, streamlining global feature extraction through voxel classification, as opposed to previous regression-based methods. In the second stage, we introduce the Occupancy Generation Network (OccGen), a conditional occupancy diffusion model based on a transformer architecture and enhanced by our Point-Voxel Fuse (PVF) block. This block integrates coarse density voxels with partial points to leverage both global and local features for comprehensive completion. By thresholding the occupancy field, we convert it into a complete point cloud. Additionally, our method employs diverse training mixtures and efficient diffusion parameterization to enable effective one-step sampling during both training and inference. Experimental results demonstrate that Diffusion-Occ outperforms existing discriminative and generative methods.

1 Introduction

With the proliferation of 3D sensor technology, point clouds have become essential for efficiently capturing three-dimensional data. However, real-world point clouds often suffer from incompleteness as a result of partial observation, self-occlusion, *etc*. This incompleteness poses significant challenges for applications such as 3D reconstruction and scene understanding, which eventually restricts their practical usability across fields such as autonomous driving, robotics, and remote sensing.

To address the challenges associated with point cloud completion, several discriminative methods have been proposed (Yuan et al. 2018; Yang et al. 2018; Xie et al. 2020; Zhou et al. 2022; Li et al. 2023; Wang et al. 2024). Most of these methods employ an encoder-decoder architecture, which excels at extracting global features from incomplete point clouds and mapping them back to the point space for completion. Despite their success, these approaches face intrinsic limitations due to their deterministic frameworks. First, while the encoder captures valuable global features from the incomplete point cloud, it inevitably loses some detailed information, leading to challenges in recovering missing parts. Second, the decoder only leverages the global features extracted by the encoder but fails to utilize the fine-grained regularization given partial points (*e.g.,* spatial regularization given by input coarse point clouds) well, which often leads to shape deformation in cloud completion. These limitations prompt researchers to explore generative frameworks for point-cloud completion.

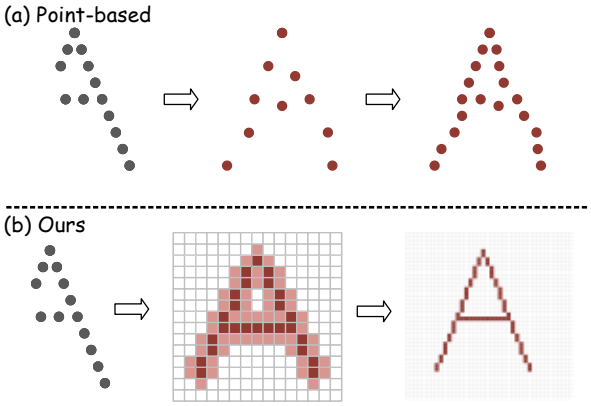

Figure 1: Comparison between previous point-based methods and our occupancy-based point cloud completion method. Previous methods focus on point regression tasks, while our approach addresses density classification tasks. We convert partial inputs into coarse density voxels, refine them into dense occupancy fields.

As a powerful and emerging generative framework, diffusion models (Ho, Jain, and Abbeel 2020) offer a robust approach to point cloud completion by iteratively refining Gaussian noise to produce uniform and high-quality point clouds. However, these methods face challenges in further improved accuracies due to the use of raw point-cloud representation in the diffusion framework. Specifically, dissimilar to the images, the point clouds are essentially irregular and

*These authors contributed equally.

unstructured, which means that the diffusion model can not well utilize the spatial structural information, *e.g.,* neighboring information, for point-cloud completion, which results in incomplete details and uneven distribution of the completed point cloud.

To address the issue, we propose replacing point-based representations with occupancy-based representations in the diffusion process (Figure 1). Unlike raw point clouds, occupancy-based representations are spatially structured, allowing diffusion models, such as U-Net (Rombach et al. 2022), to effectively utilize spatial information from coarse input point clouds for improved completion. Additionally, determining the occupancy status of a region is inherently simpler than predicting individual point positions, which enhances prediction accuracy. Voxels, with their well-defined structure, are less susceptible to significant deformation during refinement, ensuring better consistency between the completed point cloud and the original incomplete input.

In particular, we propose an innovative framework **Diffusion-Occ** that recovers the complete point clouds with dense occupancy fields as intermediate representations. Diffusion-Occ employs a novel two-stage coarse-to-fine strategy that overcomes the limitations of the traditional diffusion model in quality and speed. We first propose Coarse Density Voxel Prediction Network (CDNet) to predict coarse density voxels, significantly easing subsequent dense occupancy field generation. These results serve as conditions for our proposed Occupancy Generation Network (OccGen) in the next stage, which integrates the previous partial inputs. Additionally, inspired by (Saxena et al. 2023), we incorporate v-prediction techniques to accelerate diffusion sampling. Our method demonstrates improvements in ShapeNet-55 across three classes, achieving at least a **+12%** improvement on Airplanes, **+4%** on Cars, and **+9%** on Chairs.

Our **key** contributions are summarized as follows:

- We present the Diffusion-Occ framework for 3D point cloud completion, utilizing a coarse-to-fine approach to effectively model occupancy distributions and preserve point cloud details.
- We introduce CDNet for reconstructing coarse shapes from incomplete point clouds and develop the innovative PVF Block to integrate global features from partial point clouds for robust completion.
- Experiments show that our method delivers outstanding performance in point cloud completion and produces visually appealing results.

2 Related Work

Discriminative-based Point Cloud Completion Methods. Discriminative methods represent the mainstream approach for point cloud completion. These methods take incomplete point clouds as input and produce their complete corresponding shapes as output. Given the unordered nature of point clouds and the success of CNNs in image processing, early point cloud completion methods often employed voxels or distance fields to represent 3D shapes. This structured approach allowed for the extraction of features from incomplete point clouds using convolutional operations, facilitating the prediction of complete shapes. However, these methods were limited by significant memory consumption and computational overhead. PointNet (Qi et al. 2017) reduced computational costs and improved performance by avoiding the information loss typically associated with quantization operations. Building on this, point-based completion methods, such as PCN (Yuan et al. 2018), adopted a coarse-to-fine two-stage completion strategy to reconstruct complete shapes, influencing subsequent methods. However, point-based methods often struggle with reconstructing fine details due to insufficient focus on local structural features. To address this, some methods introduced more complex feature extractors and training strategies to improve model performance. For instance, GRNet (Xie et al. 2020) integrates point clouds with voxels and uses 3D convolution to extract local shape features. Recently, the Transformer (Vaswani et al. 2017) architecture has been widely applied to point clouds, leveraging its ability to model long sequences and handle dependencies between points effectively. PointTr (Yu et al. 2021) was the first to apply the Transformer architecture to point cloud completion, with its geometry-aware Transformer module modeling local point relationships and enabling global information exchange between neighborhoods, achieving notable performance improvements. Expanding on this, SeedFormer (Zhou et al. 2022) enhances point generation by integrating spatial and semantic relationships among neighboring points, while ProxyFormer (Li et al. 2023) introduces Proxy Alignment, transforming missing parts into proxies and refining predictions iteratively using prior knowledge. Our approach also follows a coarse-to-fine architecture, with the first stage, CDNet, focusing on coarse density voxel prediction compared to previous coarse point prediction methods.

Generative-based Point Cloud Completion Methods. Generative methods, such as GANs (Goodfellow et al. 2014), Flow (Rezende and Mohamed 2015), and Autoencoders (Kingma and Welling 2013), offer an alternative approach to 3D point cloud completion by generating diverse and plausible global shapes based on partial inputs. Specifically, l-GAN (Achlioptas et al. 2018) employs GANs trained on point clouds and latent variables, PointFlow (Yang et al. 2019) utilizes continuous normalizing flows within a probabilistic framework, and SetVAE (Kim et al. 2021) leverages a hierarchical variational autoencoder for sets, incorporating latent variables to manage coarse-to-fine dependencies and permutation invariance. Despite their strong generative capabilities, these methods often struggle to achieve high accuracy compared to ground truth. Diffusion models (Ho, Jain, and Abbeel 2020; Peebles and Xie 2023), which have demonstrated superior performance in image generation, are now being adapted for 3D generation and completion tasks. For instance, Luo et al.(Luo and Hu 2021) introduced DDPM for unconditional point cloud generation using Pointwise-net, though challenges remain in generating fine-grained local structures. Zhou et al.(Zhou, Du, and Wu 2021) applied conditional DDPM for point cloud completion using a point-voxel CNN approach. LAS-Diffusion (Zheng et al.

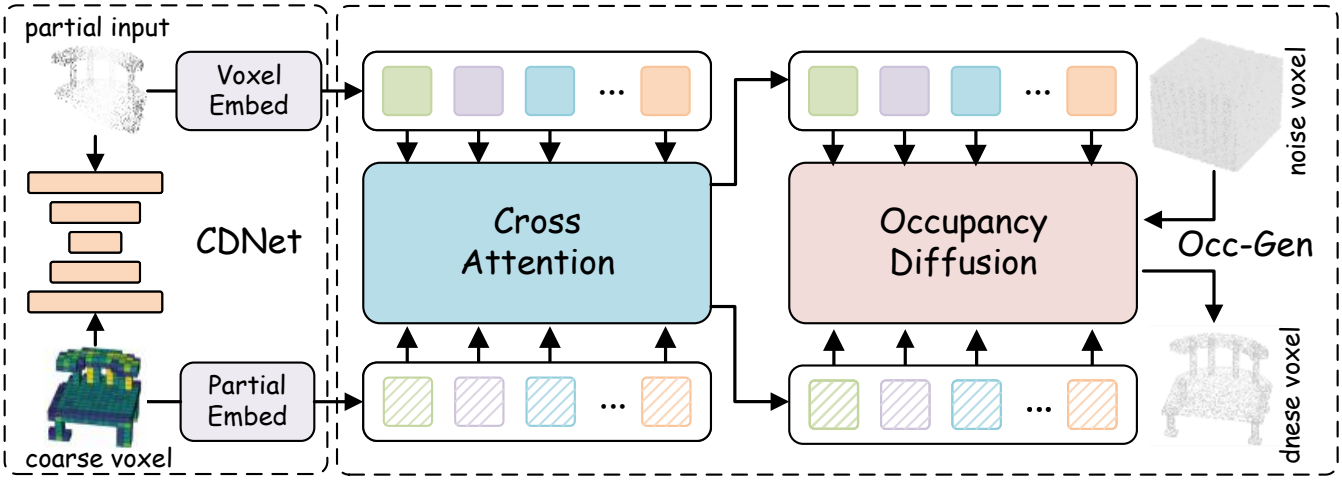

Figure 2: The Diffusion-Occ model consists of two stages: the coarse stage (CDNet) and the fine stage (OccGen). In the coarse stage, CDNet predicts coarse density voxels. It processes partial points of size $M \times 3$, voxelizes them, and uses a 3D U-Net to generate a coarse density voxel grid of size $v \times v \times v$. In the fine stage, these coarse density voxels are processed by an embedding layer to produce voxel tokens. A separate partial embedding layer generates point tokens. Cross-attention is then applied between the voxel tokens and point tokens to aggregate global and local details. OccGen leverages these tokens to transform noise signals into dense occupancy fields of size $u \times u \times u$ using a transformer-based network. This network efficiently integrates both point and voxel features through cross-attention and adaptive instance normalization.

2023) improved 3D object generation through two-stage model training and a novel view-aware local attention mechanism for better local control and model generalization. DIT-3D (Mo et al. 2024) introduced the Diffusion Transformer architecture for 3D shape generation, and DiffComplete (Chu et al. 2024) achieved high completion accuracy and diversity through hierarchical and spatially-consistent feature aggregation in conditional generation. Distinctively, our approach employs an occupancy-based diffusion model for point cloud completion, conditioning on both partial points and coarse density voxels enriched with global features. Our coarse-to-fine strategy enhances accuracy, while our novel diffusion parameterization improves sampling efficiency, reducing surface artifacts and enhancing the realism of the completed 3D points.

3 Method

In this section, we define the task of completing partial 3D point clouds using our novel occupancy diffusion framework, Diffusion-Occ. Our approach employs a two-stage coarse-to-fine strategy. First, we present Coarse Density Voxel Prediction Network (CDNet), which predicts coarse density voxels (see Section 3.1 for details). Next, we describe Occupancy Generation Network(OccGen), which generates an occupancy field conditioned on partial points and the coarse density voxels (discussed in Section 3.2).

3.1 Coarse Density Voxel Prediction Network

Overview. Our CDNet module is designed to convert the partial point cloud P into coarse density voxels V, which correspond to the complete point cloud Q. In the following sections, we will detail the creation of ground-truth density voxels and the network architecture.

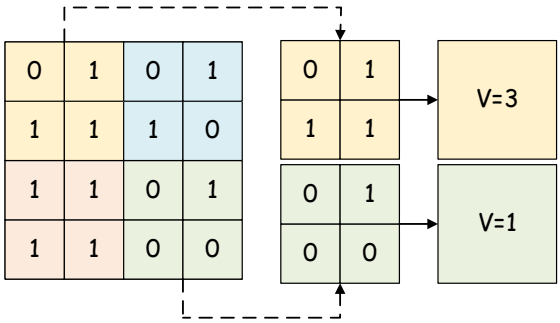

Figure 3: Illustration of the coarse density voxel calculation method on a two-dimensional plane. If a coarse voxel is occupied by one child, the value is 1; if occupied by three children, the value is 3.

Voxelization. We introduce the concept of coarse density voxels, as depicted in Figure 3. The value of a voxel v is determined by the count of occupied nodes among its child subspaces. Additionally, we first convert the input incomplete point cloud P into the corresponding voxelized point cloud PV:

$$PV_{u,v,w} = \frac{1}{N_{u,v,w}} \delta \left[\lfloor x \times r \rfloor = u, \right. \\ \left. \lfloor y \times r \rfloor = v, \lfloor z \times r \rfloor = w \right] \times (x, y, z), \tag{1}$$

where r denotes the voxel resolution, and δ is a binary indicator determining whether a point $p = (x, y, z)$ belongs to the voxel grid (u, v, w). We use PV as input to predict the coarse density voxel V.

Network Architecture. The module is based on a standard 3D U-Net architecture. The encoder consists of four layers that progressively reduce the voxelized point size from 12^3 to 6^3, 3^3, and finally 1^3, with the number of channels decreasing from 1 to 8, 64, and 512, respectively. The decoder restores the resolution to the original size. Skip connections are used to minimize information loss. A classification head is applied to the voxelized output. This voxelized point cloud allows us to efficiently extract information from incomplete point clouds and aligns directly with our coarse voxel representation. We then feed the voxelized point cloud PV into a 3D U-Net for feature extraction:

$$F = \text{UNet}(PV), \tag{2}$$

For each $PV_i \in PV$, its corresponding feature F_i is input into a classification head to predict its assigned category:

$$\text{Occ}_i = \text{MLP}(F_i). \tag{3}$$

Network Training. Unlike previous methods that predict spatial coordinates for coarse point clouds, our CDNet predicts the occupancy category for each voxel, thereby transforming a continuous regression problem into a discrete classification problem. Predicting categories is more straightforward and robust compared to predicting spatial positions. At this stage, our model aims to minimize the cross-entropy loss:

$$L = -\frac{1}{N}\sum_{i=1}^{N}\sum_{c=1}^{C} y_{i,c}\log(\hat{y}_{i,c}), \tag{4}$$

where C represents the total number of categories, which is 9, ranging from 0 to 8.

3.2 Occupancy Generation Network

Overview. To improving point completion results, we use the OccGen module to refine the coarse density voxels obtained in the previous stage, generating dense occupancy fields. After generation, we can derive the completed point cloud via binarization. Here, we will detail how to utilize the coarse density voxels for conditional generation and introduce the Point-Voxel Fuse Block (PVF Block) and v-parameterization, along with our training strategy.

Network Architecture. Figure 2 provides an overview of our network architecture, which includes a preprocessing module and a conditional fusion module. The preprocessing module converts partial points and coarse density voxels into point tokens c_p and voxel tokens c_v using embedding layers. These tokens then undergo cross-attention to produce updated point and voxel tokens. Subsequently, the noise volume is passed through a patchify layer to obtain embeddings x_t. The patchify operation converts the original $1 \times u \times u \times u$ volume into $np \times h$ tokens, where np represents the number of patches with size u^3/p^3 and h is the hidden dimension, with p being the patch size. The embeddings x_t are iteratively processed through the PVF block as follows:

$$x_t^i = \text{PVF}^i(x_t^{i-1}, c_p, c_v), \quad i = 1, 2, \ldots, m \tag{5}$$

The final output from the last PVF block is passed through an unpatchify layer to produce a $1 \times u \times u \times u$ dense occupancy volume. During inference, a threshold is applied to the occupancy fields to convert them into points, resulting in the completion of points.

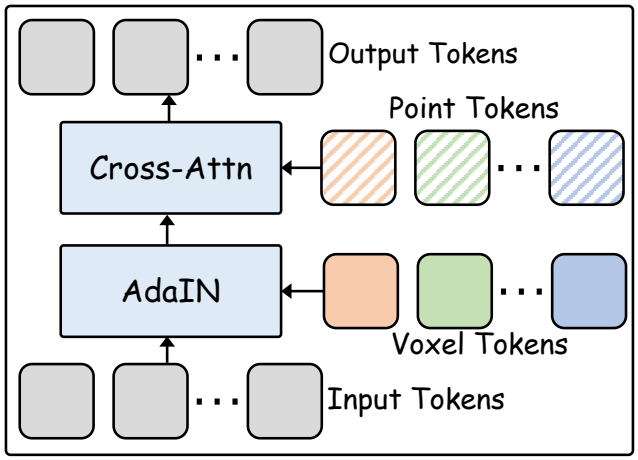

Figure 4: Overview of our Point-Voxel Fuse Block. The input consists of noise volume embeddings, with dimensions $B \times N \times H$, where B is the batch size, N is the number of input tokens, and H is the feature dimension. Both point tokens and voxel tokens have dimensions $B \times n \times H$ (with $n \ll N$). First, the input tokens undergo Adaptive Instance Normalization with the voxel tokens to aggregate global information. Then, cross-attention is applied with the point tokens to capture local details. The output tokens maintain the same dimensions as the input tokens.

Point-Voxel Fuse Block. To further integrate point tokens c_p and voxel tokens c_v with the occupancy field x_t, we designed a specialized block, the Point-Voxel Fuse (PVF) block. Figure 4 illustrates the conditional fusion process. The input consists of noise volume embeddings x_t with dimensions $B \times N \times H$, where B is the batch size, N is the number of input tokens, and H is the feature dimension. Both point tokens and voxel tokens have dimensions $B \times n \times H$ (with $n \ll N$). First, Adaptive Instance Normalization (AdaIN) is applied to the input tokens using the voxel tokens to aggregate global information. AdaIN is formulated as:

$$\text{AdaIN}(x_t, \gamma, \beta) = \gamma\left(\frac{x_t - \mu(c_v)}{\sigma(c_v)}\right) + \beta, \tag{6}$$

where x_t represents the input tokens, $\mu(c_v)$ and $\sigma(c_v)$ are the mean and standard deviation of the voxel tokens c_v, respectively, and γ and β are learnable parameters. Next, cross-attention is applied with the point tokens to capture local details. The output tokens maintain the same dimensions as the input tokens. Cross-attention can be formulated as:

$$\text{Cross-Attention}(Q, K, V) = \text{softmax}\left(\frac{QK^\top}{\sqrt{d}}\right)V, \tag{7}$$

where Q, K, and V represent the query matrix derived from the updated x_t, the key matrix, and the value matrix from the point tokens c_p, respectively, and d is the dimensionality of the hidden space. This design allows us to hierarchically incorporate conditional features, leveraging both lo-

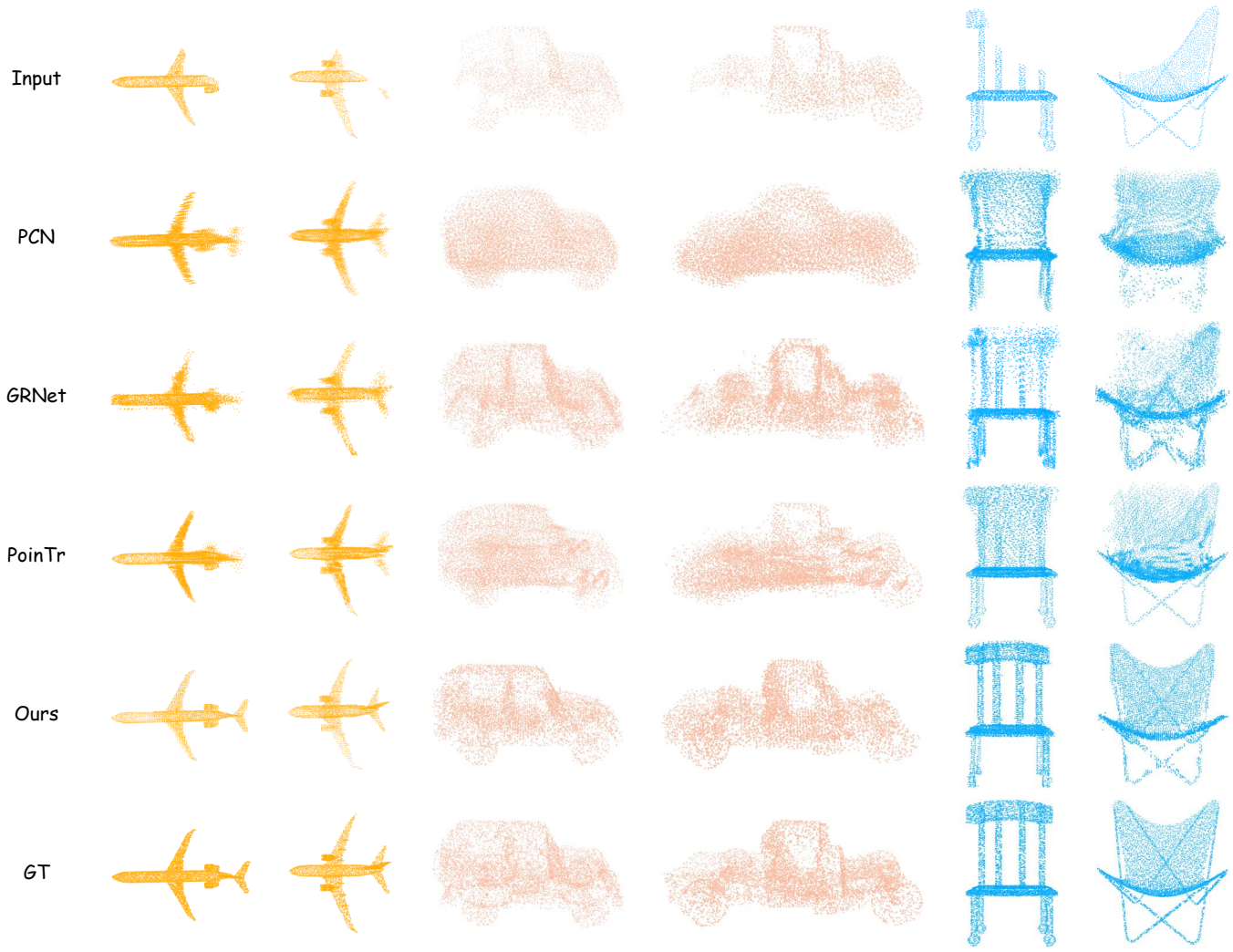

Figure 5: Visualization of 3D point cloud completion results for Airplanes, Cars, and Chairs. Compared to previous methods such as PCN (Yuan et al. 2018), GRNet (Xie et al. 2020), and PoinTr (Yu et al. 2021), our method achieves the highest quality of completion.

cal and global contexts to optimize network outputs. Aggregating features solely from point tokens might miss global accuracy, potentially reducing completion precision due to limited contextual information. Conversely, aggregating features only from voxel tokens might miss local details, which can also compromise completion accuracy. Further ablation studies are provided in Sec. 4.3.

v-parameterization. Our approach utilizes the v-parameterization (Salimans and Ho 2022). In this parameterization, the denoising network operates on a noisy target occupancy voxel $\mathbf{x}_t = \alpha_t \mathbf{x}_0 + \sigma_t \epsilon$, where $\mathbf{x}_0$ represents the clean target input (occupancy voxel, with discrete values of 1 for occupied and -1 for free), $\epsilon \sim \mathcal{N}(0, I)$, $t \sim \mathcal{U}(0, 1)$, $\alpha_t^2 + \sigma_t^2 = 1$, and $\alpha_t > 0$ follows a predefined noise schedule. Unlike the ϵ-parameterization, the denoising network predicts $v_t \equiv \alpha_t \epsilon - \sigma_t \mathbf{x}_0$. The training loss is computed as the L1 loss between the network's output $v_\theta(\mathbf{x}_t, c, t)$, where c represents an optional conditioning signal (such as coarse density voxels and partial points), and v_t. During inference, the estimate of $\mathbf{x}_0$ is derived as $\hat{\mathbf{x}}_0 = \alpha_t \mathbf{x}_t - \sigma_t v_\theta(\mathbf{x}_t, c, t)$. Following DDIM (Song, Meng, and Ermon 2020), $\hat{\mathbf{x}}_0$ can be used to derive $\hat{x}_s$ for $s < t$. After sampling, the final $\mathbf{x}_0$ is thresholded, with values greater than 0 considered occupied, and subsequently devoxelized into points.

Diffusion Training Strategy. Regarding training schemes, we have observed that a linear noise schedule outperforms a cosine schedule. During practical implementation, we transform v_t, predicted by v-prediction, into $\hat{\mathbf{x}}_0$. Due to the sparsity of occupancy, we automatically select a mask based on a threshold. Only regions where the occupancy is greater than 0 (i.e., occupied points) contribute to the L1 loss. Additionally, aside from the L1 loss, we impose a binary classifica-

tion constraint on $\hat{\mathbf{x}}_0$. The overall loss L is formulated as:

$$L = \lambda L_1 + (1 - \lambda) L_{\text{bce}} \tag{8}$$

where L_1 denotes the L1 loss, L_{bce} represents the binary cross-entropy loss for the classification constraint on $\hat{\mathbf{x}}_0$, and λ is a balancing parameter. In practice, λ is set to 0.3.

4 Experiments

4.1 Experimental Setup

Datasets and benchmarks. Combining insights from recent generative (e.g., (Zhou, Du, and Wu 2021; Vahdat et al. 2022; Mo et al. 2024)) and discriminative works (e.g., (Yu et al. 2021; Wang et al. 2024)), we utilize ShapeNet-55 (Chang et al. 2015) datasets (Airplanes, Cars, Chairs) for 3D point cloud completion. We adopt an 80-20 split, randomly selecting 80% for training and the rest for evaluation. Each object's point cloud consists of 8,192 surface points from 8 viewpoints. During training, we use 2,048 points as input and aim to reconstruct 8,192 points. The incompleteness level n varies from 2,048 to 6,144 points (25% to 75% completeness). For evaluation, we fix 8 viewpoints and set n to 2,048, 4,096, or 6,144 points (25%, 50%, or 75% completeness), categorizing results into *simple*, *moderate*, and *hard* difficulty levels. Results will include per-level performance metrics and an average (*Avg*) across all levels. Input partial point clouds are consistently down-sampled to 2,048 points during training and inference.

Evaluation Metrics. Following established practices (Yu et al. 2021; Zhou et al. 2022), we employ the mean Chamfer Distance (CD) as our evaluation metric to quantify the set-level distance between predicted point clouds and ground-truth. The Chamfer Distance between the prediction point set $\mathcal{P}$ and the ground-truth point set $\mathcal{G}$ is computed as:

$$\text{CD}(\mathcal{P}, \mathcal{G}) = \frac{1}{|\mathcal{P}|} \sum_{p \in \mathcal{P}} \min_{g \in \mathcal{G}} \|p - g\|_2^2 + \frac{1}{|\mathcal{G}|} \sum_{g \in \mathcal{G}} \min_{p \in \mathcal{P}} \|p - g\|_2^2 \tag{9}$$

Implementation Details. Our implementation is based on the PyTorch framework (Paszke et al. 2019). We employed a two-stage coarse-to-fine approach for training. In the first stage, the partial points M are set to 2048, and the final complete points N are 8192. For training CDNet in the first stage, we used 100 epochs with a batch size of 64. The AdamW optimizer was applied with an initial learning rate of 0.0002, and the WarmUp Cosine learning rate scheduler was employed. The coarse density voxel size is $12 \times 12 \times 12$. In the second stage, for training OccGen, we used 200 epochs with a batch size of 16. The same AdamW optimizer and WarmUp Cosine learning rate scheduler were used, with an initial learning rate of 0.0002. The input occupancy size was $72 \times 72 \times 72$, with a patch size of 8 and a total number of patches 9^3, and a hidden dimension of 768. Both point tokens and voxel tokens have a length of 128. The PVF Block was stacked 24 layers deep. All experiments were conducted on a system equipped with four 24GB RTX 3090 GPUs.

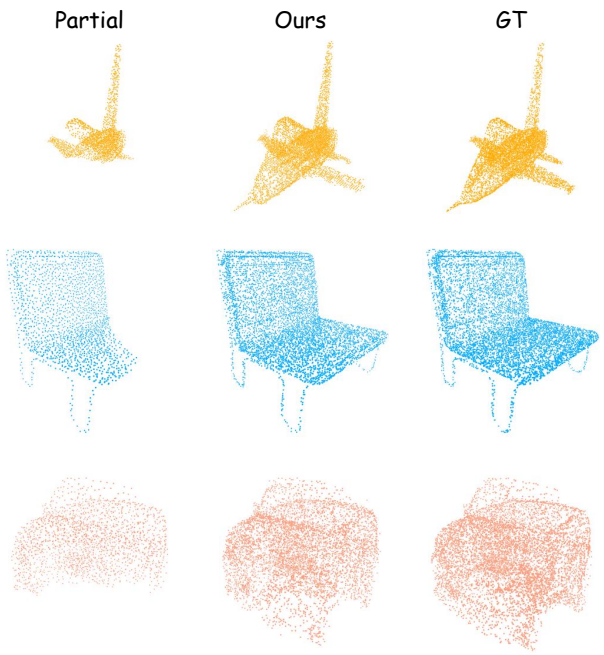

Figure 6: Completion results of Diffusion-Occ for various levels of occlusion on Airplanes, Cars, and Chairs.

4.2 Main Results

Quantitative Results. On the ShapeNet-55 benchmark, we focused on three classes (Airplanes, Cars, Chairs). We compared Diffusion-Occ against state-of-the-art (SOTA) discriminative methods (Yuan et al. 2018; Xie et al. 2020; Yu et al. 2021; Zhou et al. 2022; Li et al. 2023) and generative methods (Zhou, Du, and Wu 2021) in terms of completion accuracy, specifically using Chamfer distance L2 errors. We evaluated pre-trained models directly where available; otherwise, we re-trained them using the baselines' provided implementations on our benchmark. For generative methods, we averaged results from five inferences, each with random initialization. The detailed comparisons are presented in Table 1. Relative to PVD (Zhou, Du, and Wu 2021), Diffusion-Occ utilizes a coarse-to-fine architecture, significantly enhancing completion accuracy. Specifically, Diffusion-Occ achieves a 55% improvement on Airplanes (0.30 vs. 0.66), 36% on Cars (0.75 vs. 1.17), and 48% on Chairs (0.74 vs. 1.42). For discriminative methods, we adhered to standard training and evaluation protocols. When compared with state-of-the-art methods like SeedFormer (Zhou et al. 2022) and ProxyFormer (Li et al. 2023), our Diffusion-Occ demonstrates robust improvements across simple, moderate, and hard completion levels. Notably, it achieves reductions of at least 12% on Airplanes (0.30 vs. 0.34), 4% on Cars (0.75 vs. 0.78), and 9% on Chairs (0.74 vs. 0.81).

Qualitative Results. In Fig. 5, we present visual comparisons of completion results across three classes (Airplanes, Cars, and Chairs) using various methods. Our approach demonstrates superior ability in accurately positioning missing points and reducing noise during refinement, resulting in more realistic and high-fidelity shapes. Notably, our method

Table 1: Detailed results on Airplanes, Cars and Chairs. *S.*, *M.*, and *H.* stand for the simple, moderate, and hard settings.

CD-ℓ_2($\times$ 1000)	Airplanes				Cars				Chairs			
	S.	M.	H.	AVG.	S.	M.	H.	AVG.	S.	M.	H.	AVG.
PCN (Yuan et al. 2018)	0.90	0.89	1.32	1.04	1.48	1.47	2.60	1.85	1.70	1.81	3.34	2.28
GRNet (Xie et al. 2020)	0.87	0.87	1.27	1.00	1.29	1.48	2.14	1.64	1.24	1.56	2.73	1.84
PVD (Zhou, Du, and Wu 2021)	0.41	0.57	0.99	0.66	0.82	1.01	1.68	1.17	0.70	1.21	2.34	1.42
PoinTr (Yu et al. 2021)	0.27	0.38	0.69	0.45	0.64	0.86	1.25	0.92	0.49	0.74	1.63	0.95
SeedFormer (Zhou et al. 2022)	0.23	0.35	0.61	0.40	0.65	0.86	1.17	0.89	0.41	0.65	1.38	0.81
ProxyFormer (Li et al. 2023)	0.21	0.28	0.54	0.34	0.61	0.69	1.03	0.78	0.40	0.61	1.48	0.83
ours	**0.19**	**0.23**	**0.49**	**0.30**	**0.58**	**0.67**	**0.99**	**0.75**	**0.36**	**0.57**	**1.28**	**0.74**

achieves more visually plausible results compared to others. For instance, in the Airplanes example in the first and second columns, other methods either fail to clearly restore the wings, engine, and tail or produce a blurry appearance. In contrast, our method accurately restores the shape with precise density. For Cars, shown in the third and fourth columns, while PCN (Yuan et al. 2018) and PoinTr (Yu et al. 2021) manage to recover the general outline, they struggle with details such as the tires and windows and tend to distribute points uniformly. Diffusion-Occ, however, accurately perceives the distribution of missing points, leading to a more realistic and coherent completion. Similarly, in the fifth and sixth columns with chairs, PCN (Yuan et al. 2018) and PoinTr (Yu et al. 2021) significantly deform the chair and leave noticeable noisy points, resulting in a blurry appearance. GRNet (Xie et al. 2020) completes some details but lacks overall point cloud perception, causing discrepancies in shape and density. Our method, on the other hand, produces a more refined chair with prominent details in the legs and backrest. Additionally, Fig. 6 showcases further visualization results of Diffusion-Occ on these classes, highlighting our method's capability in point cloud completion.

4.3 Ablation Study

In this section, we conducted ablation studies to demonstrate the benefits of integrating three primary 3D design components (PVF Block, CE loss, and v-prediction) in 3D point cloud completion. All experiments were validated using the airplane category under the simple setting.

Table 2: Ablation studies on PVF block and training loss. P denotes partial points, V denotes coarse density voxels.

Ablation: PVF	CD-ℓ_2
Only P	0.38
Only V	0.25
With PVF	0.19

Ablation: Loss	CD-ℓ_2
L1 w/o mask	0.45
L1 with mask	0.23
L1 with mask + BCE	0.19

Ablation Study on PVF Block. The purpose of our experiment is to validate the effectiveness of the point-voxel fuse (PVF) block. As shown in Table. 2, when considering only partial points passed through a simple embedding layer, the CD-ℓ_2 error on airplanes is reduced to 0.38. Introducing coarse density voxels independently lowers this error further to 0.25, as these voxels enhance overall model predictions and partially alleviate the learning difficulty for OccGen. Combining partial points with coarse density voxels, which integrates both global and local features, achieves the best performance with a CD-ℓ_2 error of 0.19.

Table 3: Comparison of CD-ℓ_2 error for different parameterizations and numbers of denoising steps.

Num Denoising Steps	ϵ	x	v
1	1.374	1.123	0.198
5	1.184	0.915	0.195
10	0.609	0.474	0.187
50	0.205	0.191	0.186

Ablation Study on Training Loss. This experiment aims to validate the effectiveness of the proposed loss functions. As shown in Table 2, the most basic loss, L1 loss without any masking, results in a CD-ℓ_2 error of 0.45. Introducing a constraint on the generated dense occupancy voxels by considering only parts where the threshold ¿ 0 significantly reduces computational overhead, enhances model performance, and accelerates convergence. This modification lowers the CD-ℓ_2 error to 0.23, a reduction of 48% (0.23 vs. 0.45). Finally, incorporating a binary cross-entropy (BCE) loss as a global constraint further improves model performance, reducing the CD-ℓ_2 error to 0.19.

Ablation Study on Diffusion Parameterization. This experiment aims to validate the effectiveness of v-prediction. Inference latency is a significant concern with diffusion models for point cloud completion, particularly with the high computational cost associated with 50 denoising steps. We observe that v-parameterization dramatically reduces the number of denoising steps needed to achieve good performance. As shown in Table 3, the ϵ-parameterization requires 50 denoising steps to match the performance of a model using v-parameterization with only 1 denoising step. Intuitively, v-prediction aggregates x-prediction and ϵ-prediction in a weighted manner, ensuring effective sampling guidance even as $\mathrm{SNR}(t)$ approaches 0, thereby maintaining signal integrity.

5 Conclusion

In this study, we introduce Diffusion-Occ, an innovative occupancy-based diffusion network designed for point cloud completion. Leveraging the 3D occupancy space, our method achieves enhanced fidelity in capturing geometric details and accurately fitting point clouds to object surfaces. To improve the accuracy of object completion, we employ a two-stage coarse-to-fine approach. In the first stage, CDNet utilizes voxel classification to estimate coarse density voxels. In the second stage, OccGen integrates information from partial points and coarse density voxels, effectively balancing global context with local detail preservation. With these advancements, we establish a new paradigm in diffusion-based approaches for point cloud completion, offering robust solutions for real-world applications requiring detailed and accurate 3D reconstructions.

References

Achlioptas, P.; Diamanti, O.; Mitliagkas, I.; and Guibas, L. 2018. Learning Representations and Generative Models for 3D Point Clouds. In *Proceedings of the International Conference on Machine Learning (ICML)*.

Chang, A. X.; Funkhouser, T.; Guibas, L.; Hanrahan, P.; Huang, Q.; Li, Z.; Savarese, S.; Savva, M.; Song, S.; Su, H.; Xiao, J.; Yi, L.; and Yu, F. 2015. ShapeNet: An Information-Rich 3D Model Repository. *arXiv preprint arXiv:1512.03012*.

Chu, R.; Xie, E.; Mo, S.; Li, Z.; Nießner, M.; Fu, C.-W.; and Jia, J. 2024. Diffcomplete: Diffusion-based generative 3d shape completion. *Advances in Neural Information Processing Systems*, 36.

Goodfellow, I.; Pouget-Abadie, J.; Mirza, M.; Xu, B.; Warde-Farley, D.; Ozair, S.; Courville, A.; and Bengio, Y. 2014. Generative adversarial nets. *Advances in neural information processing systems*, 27.

Ho, J.; Jain, A.; and Abbeel, P. 2020. Denoising diffusion probabilistic models. *Advances in neural information processing systems*, 33: 6840–6851.

Kim, J.; Yoo, J.; Lee, J.; and Hong, S. 2021. SetVAE: Learning Hierarchical Composition for Generative Modeling of Set-Structured Data. In *Proceedings of the IEEE/CVF Conference on Computer Vision and Pattern Recognition (CVPR)*, 15059–15068.

Kingma, D. P.; and Welling, M. 2013. Auto-encoding variational bayes. *arXiv preprint arXiv:1312.6114*.

Li, S.; Gao, P.; Tan, X.; and Wei, M. 2023. Proxyformer: Proxy alignment assisted point cloud completion with missing part sensitive transformer. In *Proceedings of the IEEE/CVF conference on computer vision and pattern recognition*, 9466–9475.

Luo, S.; and Hu, W. 2021. Diffusion probabilistic models for 3d point cloud generation. In *Proceedings of the IEEE/CVF conference on computer vision and pattern recognition*, 2837–2845.

Mo, S.; Xie, E.; Chu, R.; Hong, L.; Niessner, M.; and Li, Z. 2024. Dit-3d: Exploring plain diffusion transformers for 3d shape generation. *Advances in Neural Information Processing Systems*, 36.

Paszke, A.; Gross, S.; Massa, F.; Lerer, A.; Bradbury, J.; Chanan, G.; Killeen, T.; Lin, Z.; Gimelshein, N.; Antiga, L.; Desmaison, A.; Kopf, A.; Yang, E.; DeVito, Z.; Raison, M.; Tejani, A.; Chilamkurthy, S.; Steiner, B.; Fang, L.; Bai, J.; and Chintala, S. 2019. PyTorch: An Imperative Style, High-Performance Deep Learning Library. In *Proceedings of Advances in Neural Information Processing Systems (NeurIPS)*, 8026–8037.

Peebles, W.; and Xie, S. 2023. Scalable diffusion models with transformers. In *Proceedings of the IEEE/CVF International Conference on Computer Vision*, 4195–4205.

Qi, C. R.; Su, H.; Mo, K.; and Guibas, L. J. 2017. Pointnet: Deep learning on point sets for 3d classification and segmentation. In *Proceedings of the IEEE conference on computer vision and pattern recognition*, 652–660.

Rezende, D.; and Mohamed, S. 2015. Variational inference with normalizing flows. In *International conference on machine learning*, 1530–1538. PMLR.

Rombach, R.; Blattmann, A.; Lorenz, D.; Esser, P.; and Ommer, B. 2022. High-resolution image synthesis with latent diffusion models. In *Proceedings of the IEEE/CVF conference on computer vision and pattern recognition*, 10684–10695.

Salimans, T.; and Ho, J. 2022. Progressive distillation for fast sampling of diffusion models. *arXiv preprint arXiv:2202.00512*.

Saxena, S.; Hur, J.; Herrmann, C.; Sun, D.; and Fleet, D. J. 2023. Zero-shot metric depth with a field-of-view conditioned diffusion model. *arXiv preprint arXiv:2312.13252*.

Song, J.; Meng, C.; and Ermon, S. 2020. Denoising diffusion implicit models. *arXiv preprint arXiv:2010.02502*.

Vahdat, A.; Williams, F.; Gojcic, Z.; Litany, O.; Fidler, S.; Kreis, K.; et al. 2022. Lion: Latent point diffusion models for 3d shape generation. *Advances in Neural Information Processing Systems*, 35: 10021–10039.

Vaswani, A.; Shazeer, N.; Parmar, N.; Uszkoreit, J.; Jones, L.; Gomez, A. N.; Kaiser, Ł.; and Polosukhin, I. 2017. Attention is all you need. *Advances in neural information processing systems*, 30.

Wang, J.; Cui, Y.; Guo, D.; Li, J.; Liu, Q.; and Shen, C. 2024. Pointattn: You only need attention for point cloud completion. In *Proceedings of the AAAI Conference on artificial intelligence*, volume 38, 5472–5480.

Xie, H.; Yao, H.; Zhou, S.; Mao, J.; Zhang, S.; and Sun, W. 2020. Grnet: Gridding residual network for dense point cloud completion. In *European conference on computer vision*, 365–381. Springer.

Yang, G.; Huang, X.; Hao, Z.; Liu, M.-Y.; Belongie, S.; and Hariharan, B. 2019. PointFlow: 3D Point Cloud Generation With Continuous Normalizing Flows. In *Proceedings of the IEEE/CVF International Conference on Computer Vision (ICCV)*, 4541–4550.

Yang, Y.; Feng, C.; Shen, Y.; and Tian, D. 2018. Foldingnet: Point cloud auto-encoder via deep grid deformation. In *Proceedings of the IEEE conference on computer vision and pattern recognition*, 206–215.

Yu, X.; Rao, Y.; Wang, Z.; Liu, Z.; Lu, J.; and Zhou, J. 2021. Pointr: Diverse point cloud completion with geometry-aware transformers. In *Proceedings of the IEEE/CVF international conference on computer vision*, 12498–12507.

Yuan, W.; Khot, T.; Held, D.; Mertz, C.; and Hebert, M. 2018. Pcn: Point completion network. In *2018 international conference on 3D vision (3DV)*, 728–737. IEEE.

Zheng, X.-Y.; Pan, H.; Wang, P.-S.; Tong, X.; Liu, Y.; and Shum, H.-Y. 2023. Locally attentional sdf diffusion for controllable 3d shape generation. *ACM Transactions on Graphics (ToG)*, 42(4): 1–13.

Zhou, H.; Cao, Y.; Chu, W.; Zhu, J.; Lu, T.; Tai, Y.; and Wang, C. 2022. Seedformer: Patch seeds based point cloud completion with upsample transformer. In *European conference on computer vision*, 416–432. Springer.

Zhou, L.; Du, Y.; and Wu, J. 2021. 3D Shape Generation and Completion Through Point-Voxel Diffusion. In *Proceedings of the IEEE/CVF International Conference on Computer Vision (ICCV)*, 5826–5835.